Journal of Magnetic Resonance 249 (2014) 135–140

Contents lists available at ScienceDirect

Journal of Magnetic Resonance

journal homepage: www.elsevier.com/locate/jmr

Communication

Gradient-free microfluidic flow labeling using thin magnetic films and remotely detected MRI

Nicholas W. Halpern-Manners [a,b], Daniel J. Kennedy [a,c], David R. Trease [a,b], Thomas Z. Teisseyre [a,d], Nicolas S. Malecek [a,e], Alexander Pines [a,b], Vikram S. Bajaj [a,b,f,*]

[a] Materials Sciences Division, E.O. Lawrence Berkeley National Lab, Berkeley, CA, USA
[b] College of Chemistry, University of California, Berkeley, CA, USA
[c] Biophysics Graduate Group, University of California, Berkeley, CA, USA
[d] Graduate Program in Bioengineering, University of California, Berkeley and University of California, San Francisco, USA
[e] College of Engineering, University of California, Berkeley, CA, USA
[f] Department of Radiology, Stanford University School of Medicine, USA

ARTICLE INFO

Article history:
Received 3 July 2013
Revised 1 August 2014
Available online 16 October 2014

Keywords:
MRI
NMR
Remote detection
Microfluidics
Flow imaging

ABSTRACT

Nuclear Magnetic Resonance (NMR) and Magnetic Resonance Imaging (MRI) may be employed as noninvasive measurements yielding detailed information about the chemical and physical parameters that define microscale flows. Despite these advantages, magnetic resonance has been difficult to combine with microfluidics, largely due to its low sensitivity when detecting small sample volumes and the difficulty of efficiently addressing individual flow pathways for parallel measurements without utilizing large electric currents to create pulsed magnetic field gradients. Here, we demonstrate that remotely-detected MRI (RD-MRI) employing static magnetic field gradients produced by thin magnetic films can be used to encode flow and overcome some of these limitations. We show how flow path and history can be selected through the use of these thin film labels and through the application of synchronized, frequency-selective pulses. This obviates the need for large electric currents to produce pulsed magnetic field gradients and may allow for further application of NMR and MRI experiments on microscale devices.

1. Introduction

Existing methods of producing intrinsically multiplexed microanalytical devices involve the assignment of unique, localizable optical signatures to the analytes of interest or to specific regions, flow pathways, or sensor media located on the device. Examples include the development of polystyrene beads implanted with quantum dots to generate unique fluorescence signatures [1], and the striping of optically distinct metals onto microrods [2]. In some cases, these signatures are based on multiple permutable elements that form an address space of many individually recognizable "bar codes" which can be used to distinguish between regions or flow pathways. Such methods rely upon a synthetic, exogenous label element or sensor that forms an adduct with the analyte and are thus difficult to integrate into existing microfluidic chips and devices. Because the adduct is usually covalent, the label cannot be altered or reset after its initial formation.

A more general solution to the problem of microfluidic labeling should have properties similar to those of an electronic register or memory. Ideally, it should also employ an intrinsic property of the fluid itself as a means of labeling, rather than requiring the use of exogenous molecules. The spin degrees of freedom of the sample fulfill these criteria, as they are addressable and resettable by NMR pulse sequences and do not generally influence the chemistry, transport, or other property relevant to the microfluidic device. Unfortunately, magnetic resonance has been difficult to combine with microfluidics, largely due to its low sensitivity when detecting small sample volumes and the difficulty of efficiently addressing individual flow pathways for parallel measurements. Recently, we have applied remotely detected MRI to resolve three-dimensional flow fields in microfluidic devices, models of microreactors, and in nanoporous materials [3–7]. These measurements overcome many of the sensitivity limitations of microfluidic MRI, but they require pulsed magnetic field gradients that are difficult to make portable, owing to the need for large electric currents which are generated using bulky electronic amplifiers. In this work, we address the narrower problem of labeling flow pathways in microchannels without attempting to resolve their internal features.

* Corresponding author at: Google Life Sciences, Google[x], Google, 1600 Amphitheatre Parkway, Mountain View, CA 94043, USA.
E-mail address: vikbajaj@gmail.com (V.S. Bajaj).

http://dx.doi.org/10.1016/j.jmr.2014.09.016
1090-7807/

In this work, we use RD-MRI and static magnetic field gradients generated by thin magnetic films to demonstrate an MRI method that provides a non-invasive combinatorial label of the flow trajectory and history in a microchannel. This technique may allow for the development of microscale NMR and MRI experiments which do not require the large hardware footprint of conventional magnetic resonance techniques.

While traditional magnetic resonance of microscale volumes of liquid is limited by poor sensitivity (due to the low filling factor of the detection coil), RD-MRI can overcome these limitations when dealing with small volumes of flowing liquid [7–10]. Conventional magnetic resonance experiments consist of two steps. First, spectroscopic or imaging information is encoded in the nuclear spin magnetization using a series of radiofrequency and gradient pulses. The oscillating magnetic field produced by the encoded spin magnetization is then detected using the same radiofrequency coil, now acting as a receiver. In a remotely detected experiment, the "encoding" and "detection" steps are separated in both time and space, with fluid flow carrying the stored information from the encoding coil to a separate, specifically optimized detection coil. By using a detection coil whose dimensions are similar to those of the features of interest, a sensitivity enhancement of several orders of magnitude can be achieved [11]. Advanced methods development and applications of this technique have been demonstrated in previously published work [11–14]. Here, we used localized magnetic fields in a remotely detected flow experiment, allowing us to selectively image small flow features and isolate individual flow channels with no need for pulsed magnetic field gradients. We further demonstrate a microfluidic logic operation which can be generalized to improve multiplexing capabilities.

The addition of small, localized fields to a microscale device can be accomplished in several ways. The most common is to apply pulsed magnetic field gradients produced by specialized imaging coils; however, this has the disadvantage of requiring large electric currents, making the hardware non-portable. Our method is inspired by the development of molecular imaging reagents incorporating microstructures that alter the local magnetic field, creating frequency-dependent contrast in MRI methods [15]. Here, thin layers of magnetic film are positioned above and below the flow pathway in a region, with a unique number of layers, and hence a unique magnetic field, in each region. In this way, frequency-selective excitation pulses can be applied to individually isolate a desired region. We first demonstrate the application of this idea to the localized imaging of selected areas of the flow. Next, we show that a series of frequency-selective pulses in a flowing system can implement flow gate operations which will only yield signal when the sequence of local magnetic environments experienced by the flowing liquid is synchronized with the sequence of pulses. Such a system of logic could allow discrimination between multiple flow pathways on a single chip by giving each a unique magnetic signature along the flow dimension and tuning the pulses to select only the pathway of interest. Such a method may be viewed as the flow analog of a "bar code".

2. Methods

2.1. Flow phantom

The selective imaging and sequential excitation experiments were performed using a homebuilt flow phantom. Fluid traveled through a 150 μm ID (360 μm OD) PEEK capillary (Idex Health & Science, Oak Harbor, WA) which was wound to form three distinct microfluidic regions, each approximately a close-packed three-turn helix of 6 mm major diameter, as illustrated in Fig. 1. The coiled capillary was cast in a thin layer of epoxy resin to prevent changes to the flow pathway. The resulting chip consisted of three regions of looped capillary, and was sandwiched between thin layers of magnetic material in order to create distinct, localized magnetic fields in each region. High-density thin film laminates consisting of Mylar sandwiched between a pair of 1 μm layers of cobalt-doped gamma-maghemite, Co-γ-Fe_2O_3, salvaged from double-sided, high-density 3.5″ floppy diskettes, proved to be ideal thin-layer magnetic materials for creating small homogeneous fields. By varying the number of layers of magnetic material, each region was given a distinct magnetic environment. The number of layers on each side of the three regions is indicated in Fig. 1, and was chosen to be non-linear with respect to the order in which fluid flow traversed the phantom. The phantom was connected with the flow system using commercially available connectors (Idex Health & Science, Oak Harbor, WA). Water flowed through the system at a constant pressure of 13.5 psi, driven by a nitrogen gas ballast system and monitored by a proportional control setup flow meter (Omega Engineering, Stamford, CT).

2.2. Experimental setup

All remote detection experiments were performed with a 7.05 T Oxford Instruments (Oxford Instruments, Oxfordshire, UK) wide bore magnet and a Varian imaging console (Varian, Palo Alto, CA). Excitation and storage pulses were applied with a 40 mm Varian volume imaging probe, while magnetic field gradients were applied using a Varian three-axis gradient system producing up to 100 G/cm on all three axes. The homebuilt remote detection probe contained a 12-turn, 360 μm ID copper solenoid detection coil encased in a cell filled with FC-43 Fluorinert (3M, Maplewood, MN) for susceptibility matching. The flow phantom was mounted to the end of the detection probe and positioned such that both the phantom and the detection coil were within the homogeneous sweet spot region of the magnet. Shimming coils were employed to maximize the homogeneity in the encoding coil. During signal acquisition, the optimum shim values for encoding were augmented with previously calibrated magnetic field gradients in order to optimize the sweet spot for the detection region.

2.3. Pulse sequences

All experiments were carried out within the framework of a remotely detected acquisition, in which encoding and detection steps are separated in time and space. The pulse sequence for the selective imaging experiment, shown in Fig. 1B, is similar to sequences described in a previous work. [7] Frequency-selective excitation was accomplished with a $\pi/2$ eSNOB pulse of 1 kHz bandwidth [16], which was tuned to excite one of the individually addressable flow regions. Two-dimensional phase encoding gradients were then applied, and were compensated to correct for unwanted velocity effects [17]. Refocusing of transverse magnetization occurred via a π spin-echo pulse, and a final $\pi/2$ pulse was applied after the proper echo delay in order to store the encoded magnetization along the z direction for transport to the detection coil, allowing the signal to decay with the longitudinal relaxation time T_1 in place of the much shorter transverse relaxation time T_2^*. The labeling thus persists for a time period of T_1. Stroboscopic detection was carried out as the encoded fluid traveled through the microcoil, yielding additional time-of-flight information. Phase cycling was employed to store each component of the magnetization and to filter out any signal from spins outside of the encoding region. The acquisition time for each free induction decay (FID) was correlated to the amount of time each fluid packet spent in the detection coil, which was approximately 60 ms. A total of 50 time-of-flight acquisitions were collected during the course of remote acquisition. The entire encoding and detection sequence

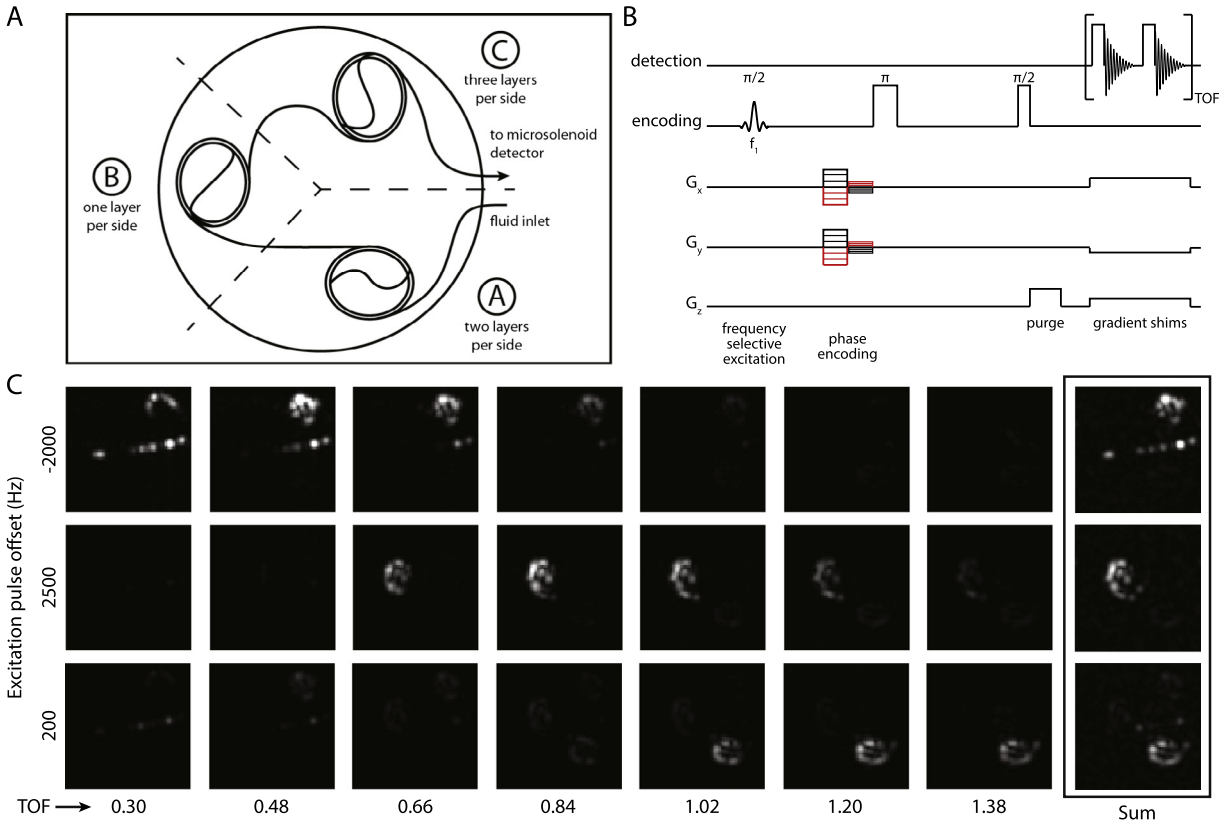

Fig. 1. (A) The imaging flow phantom. Water travels through capillary tubing which is wound to form coils in three distinct magnetic field regions, formed using varying numbers of layers of magnetic material. (B) The remote detection pulse sequence. Frequency-selective excitation excites water in one of the flow regions. Two-dimensional phase encoding gradients are applied and refocusing of transverse magnetization occurs via a π spin-echo pulse. A final $\pi/2$ pulse stores the encoded magnetization along the z direction for transport to the detection coil. Finally, stroboscopic pulses are applied with the detection coil to detect the encoded magnetization. (C) Time-of-flight and sum images illustrating the ability to selectively image each of the three flow regions by varying the excitation pulse offset frequency.

was repeated for each k-space point of the image. In this case, we acquired 31 × 31 transverse images with a field of view of 3.88 cm and a resolution of 125 μm in the x and y dimensions.

The pulse sequences for the two- and three-loop sequential excitation experiments, shown in Fig. 2, replaced the encoding portion with a series of pulses separated by time delays to allow for fluid travel between regions. Each excitation consisted of a broadband $\pi/2$ pulse followed immediately by a frequency-selective $\pi/2$ eSNOB pulse of 1 kHz bandwidth. As a result, only magnetization at the selected frequency (and thus, the selected region) was returned to z. All remaining transverse magnetization was dephased by a gradient along z during the inter-region travel delay. The frequency-selective pulses and receiver stroboscopic pulses were phase-cycled (in 4- and 8-step cycles for the two- and three-loop experiments, respectively) to yield a net positive signal for spins that survived all of the excitation steps. Detection was carried out using the method described above.

2.4. Data processing

All data were processed using MATLAB (Mathworks, Natick, MA). The direct (FID) dimension was apodized and Fourier transformed for all experiments. For the selective imaging experiments, the resulting spectra were integrated across the linewidth of the water resonance, yielding complex-valued data points for the indirect phase-encoded dimensions of the experiment. These dimensions were then apodized by Gaussian functions centered at the origin of k-space, zero-filled by a factor of 2, and transformed by a multidimensional Fourier transform to obtain complex images across the time-of-flight dimension. Summation of these images yielded an image representing the entire volume of encoded fluid.

An additional summation was carried out across the time-of-flight dimension in all sequential excitation experiments to obtain a full image of the phantom. The two-loop sequential excitation experiments also included an array across the inter-region travel delay. Integration across the direct spectral dimension yields signal intensities at each point in this array. In the three-loop experiment, the two inter-region travel delays were fixed, and the spectra are shown without integration.

3. Results and discussion

3.1. Selective imaging

RD-MRI was performed on a flow phantom consisting of a capillary wound into three distinct flow regions (Fig. 1A). Each region was sandwiched with a unique number of thin magnetic film layers, creating localized and individually addressable magnetic fields. A direct spectrum (averaged) of the flow phantom determined the spectral offset for each additional pair of layers (above and below the chip) to be approximately 2.5 kHz. The three regions, labeled A, B, and C in the order of flow, had two, one, and three layers of film on each side, respectively. By applying a standard RD-MRI sequence with a narrow band frequency selective eSNOB excitation pulse (Fig. 1B), we were able to selectively image fluid residing in each of the three regions at the time of encoding. A representative selection of the time-of-flight images and the corresponding sum images are shown in Fig. 1C. As shown, each region may be selec-

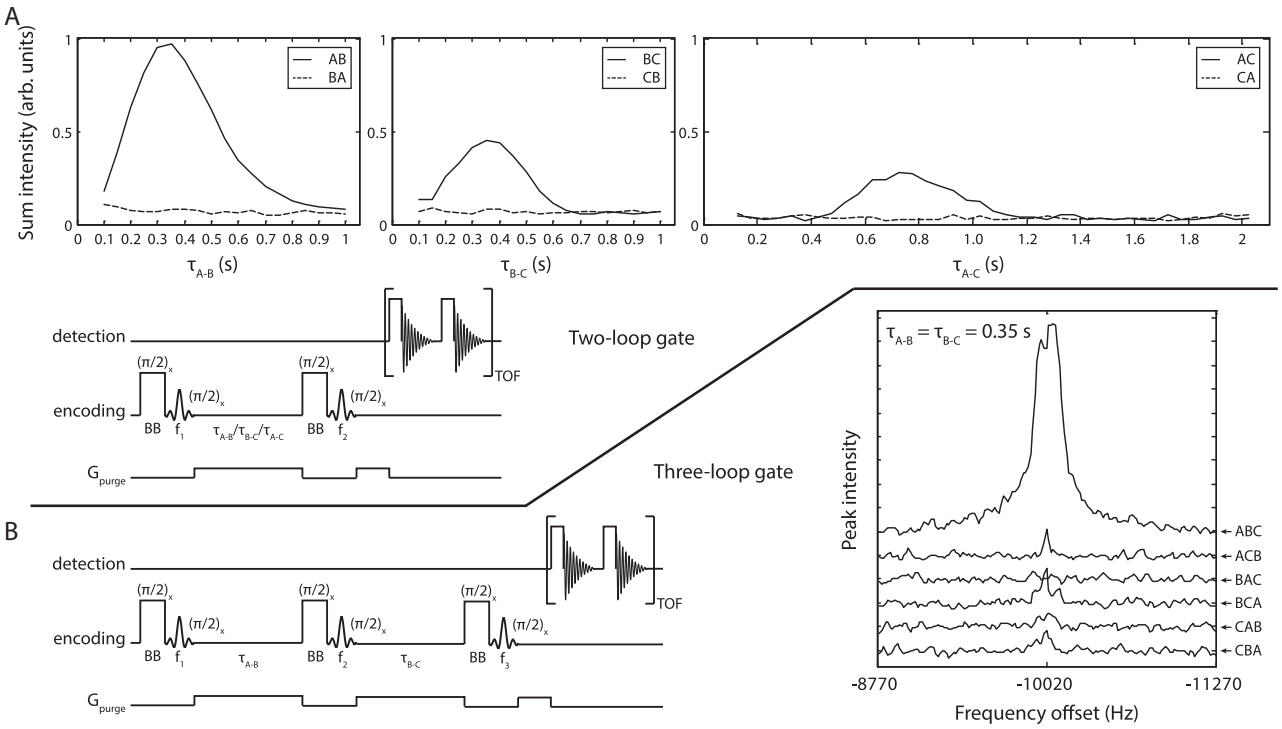

Fig. 2. (A) Two-loop sequential excitation. Sequential excitation which aligns with flow direction (i.e. AB, BC, AC) yields measurable travel curves with maximum intensity at τ_{AB} = 0.35 s, τ_{BC} = 0.35 s, and τ_{AC} = 0.70 s. When excitation ordering is inverted (i.e. BA, CB, CA), no signal is obtained. The two-loop gate for sequential excitation is shown below. (B) Three-loop sequential excitation. Remotely-detected spectra (integrated across the time-of-flight dimension) are shown for all possible permutations of three-loop sequential excitation (i.e. ABC, ACB, BAC, BCA, CAB, CBA), with two-loop travel times set at τ_{AB} = 0.35 s and τ_{BC} = 0.35 s. Appreciable signal can only be observed when the selective pulse frequencies follow the order of flow (ABC). The three-loop gate for sequential excitation is shown at bottom left.

tively imaged simply by varying the frequency of the excitation pulse. The resonance frequencies of each region were determined either by running an array of travel curves or low-resolution images. The bandwidth and shape of the pulse may be further optimized to minimize excitation overlap between regions of similar frequency. In the images of loop C, the signal outside of the loop is from the inlet capillary, which extended outside of the chip and did not have a controlled magnetic environment. The frequency of this signal could be easily shifted via shimming or removed with an alternate phantom design, but its presence here does not interfere with our initial experiments.

3.2. Sequential excitation

Frequency-selective excitation allows for experiments which use the magnetic environment of the flow pathway as a means of spatial selectivity. To demonstrate this concept in our phantom, we applied a series of frequency-selective pulses with delays corresponding to the estimated inter-region travel time. As shown above, the three regions of this phantom can be individually addressed, allowing us to perform selective two- and three-loop "gating" operations. As shown in the pulse sequences in Fig. 2, each excitation consists of a broadband $\pi/2$ pulse followed by a frequency-selective $\pi/2$ eSNOB pulse. The net effect of these pulses (and the subsequent crush z gradient during the delay) is to ensure that the only surviving magnetization is from spins which were in the correct region during each of the corresponding frequency-selective pulses. Data from the three possible pairs (AB, BC, and AC) are shown in Fig. 2. For each, the timing of the inter-region travel delay has been incremented, and all other dimensions (time-of-flight and spectral) have been summed to give a signal magnitude for each point in the travel time array. Each plot shows data from an experiment with the pulses applied in the order of flow (solid line) and one in the opposite order (dashed line). The resulting curves demonstrate the ability to selectively obtain signal based on the flow pathway, while the arrayed delay gives a quantitative measure of the travel time between regions. The signal maxima for these experiments are found at τ_{AB} = 0.35 s, τ_{BC} = 0.35 s, and τ_{AC} = 0.70 s. A selective three-loop experiment may also be performed, as shown at the bottom of Fig. 2. Here, the inter-region travel delays are fixed to give maximum signal (τ_{AB} = τ_{BC} = 0.35 s) and the spectra are shown before integration. Signal can only be observed when the selective pulse frequencies follow the order of flow (ABC); the five other permutations do not yield any detectable signal.

3.3. Imaging optimization considerations

We have developed this technique with the ultimate goal of allowing microscale NMR and MRI experiments which do not require large and non-portable imaging hardware. In addition to the proof-of-principle experiments presented above, we have conducted a computational analysis of the limitations of our technique. The hysteresis curve of a 4 mm × 5 mm piece of the floppy diskette material described above was obtained using a superconducting quantum interference device (SQUID) magnetometer at magnetic fields up to 7 T. The resulting magnetization curve was imported into the Magnetic Fields, No Currents module of the COMSOL Multiphysics software (COMSOL Group, Stockholm, Sweden). The phantom described above was modeled to test agreement of the simulations with our experimental results. In general, the NMR frequencies and linewidths obtained in the simulation agreed with experimental data to within 5%. To determine the potential one-dimensional imaging resolution, we modeled the frequency response of a 1 pL voxel of water, which is of the order of magnitude of the smallest volume of water that we expect to

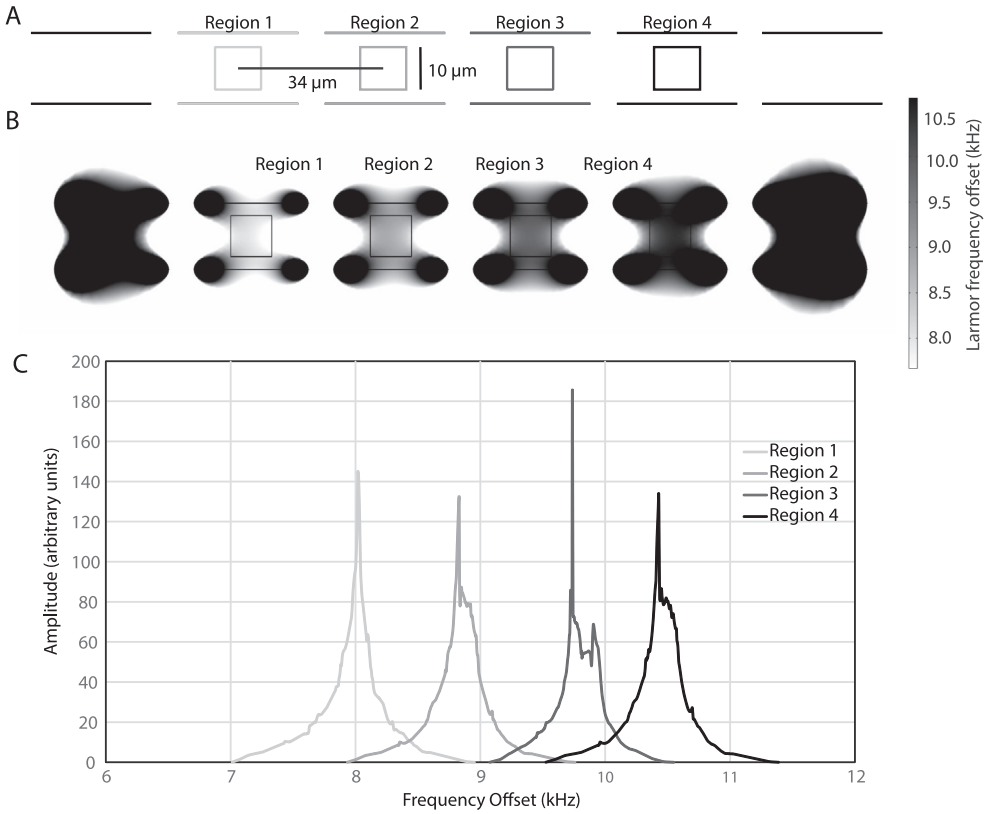

Fig. 3. (A) Cross-section of the one-dimensional array simulation. Regions of distinct magnetic field are created using thin magnetic films of varying thickness. A 1 pL volume of water is placed between two of these films. Additional films are placed to the sides of the outer regions to suppress tailing in the frequency distribution of these regions. (B) Spatial distribution of NMR resonance frequencies generated by this geometry. (C) NMR signals of each region.

be able to detect in a single-shot NMR experiment using a microcoil detector. As the ultimate goal of this research is to allow for the development of portable NMR and MRI experiments, we conducted these simulations at the lower field of 1.5 T, which is easily reached by high-resolution NMR magnets made from small Halbach arrays of permanent magnetic materials [18–20]. We simulated a line of these voxels surrounded by Pyrex glass, which was taken to be a representative construction material for a microfluidic device. We placed the voxels near thin magnetic films of Co-γ-Fe_2O_3 of varying thicknesses and optimized the frequency response by varying the geometry of the voxel, extent of the film, film thickness, and spacing of the voxels. We modified these values until the NMR signals from each voxel of water were well-resolved. Here, this is taken to mean that the tails in the NMR signals from each neighboring region did not overlap to greater than 10% of the peak height.

We were able to resolve the water signals from the various regions when using cubic voxels 10 μm on a side, with thin magnetic films placed 3 μm above and below each region. The thin films were rectangular prisms 28 μm on a side and ranged in thickness from 120 nm to 140 nm thick. The regions were separated by a center-to-center distance of 34 μm. To suppress frequency tailing behavior in the two outer regions, we placed additional thin magnetic films on the ends of the simulation. This geometry is shown in Fig. 3A. The spatial distribution of NMR resonances frequencies is shown in Fig. 3B. The resultant NMR signals for each water voxel are shown in Fig. 3C. Here, we see that the various regions display a center-to-center frequency difference of approximately 800 Hz and a FWHM linewidth of approximately 300 Hz. We note the presence of extensive tailing in the low-intensity portion of the NMR signal, which limits the spatial resolution using this geometry. We conclude that this technique is able to achieve one-dimensional spatial resolutions of 34 μm. We note that this resolution should be taken as an upper bound on the achievable resolution, as it may be possible to get better results by using different thin film geometries or different magnetic materials. We defer an exhaustive analysis of these considerations to future work.

We do not expect substantial broadening of the NMR signal due to a mismatch in the magnetic susceptibilities of water and Pyrex glass at these fields. As such, we have not conducted an extensive study of the susceptibility-induced broadening in our simulations. In the event that such broadening degrades the NMR signal to an unacceptable extent, it may be possible to utilize alternative materials which have a magnetic susceptibility closer to that of water or another solvent. Such an approach has been employed at higher magnetic fields and includes the production of susceptibility-matched NMR tube inserts [21] as well as NMR tubes made out of susceptibility-matched glasses [22]. Such techniques might be adapted to a microfluidic device which operates according to the principles described in this work. We also note that such techniques may allow for additional improvement in the lineshapes of the NMR signals attained in the various imaging regions, and further improve the attainable imaging resolution. We once again defer an analysis of these effects to future optimization studies.

4. Conclusions

We demonstrate a proof of concept experiment that allows multiplexed spatial encoding and logic in a microfluidic device without the use of pulsed magnetic field gradients. The method uses localized magnetic fields and narrow-band frequency selective pulses to perform region- and path-selective experiments with no additional electrically controlled magnetic field gradients. It

may be useful in high-throughput microfluidic assays in portable devices, where electrically controlled gradients are difficult to implement, and it may also be useful as an addressing mechanism in microfluidic logic systems, such as those based on bubble logic. We have undertaken an analysis of the limitations of this method and found that it should be capable of imaging resolutions better than 34 μm with properly optimized thin film geometries and judicious choice of magnetic materials. We envision that this technique may be applied in a microfluidic "bar code" experiment. In such an experiment, flow on the chip, or an auxiliary labeling unit, would be labeled by frequency-selective pulses and a uniquely ordered set of magnetic environments. In this manner, spatial and flow selectivity could be accomplished without the need for switched magnetic field gradients. In our proof-of-principle experiment, three different magnetic fields and three encoding regions could provide labels for up to 27 different flow pathways. Additional magnetic fields and encoding regions would increase the number of labels exponentially.

Acknowledgments

This work was supported by the U.S. Department of Energy, Office of Basic Energy Sciences, Materials Sciences and Engineering Division, under Contract No. DE-AC02-05CH11231.

References

[1] A. Couzis, S.V. Vaidya, M.L. Gilchrist, C. Maldarelli, Spectral bar coding of polystyrene microbeams using multicolred quantum dots, Anal. Chem. 79 (22) (2007) 8520–8530.
[2] S.R. Nicewarner-Peña, R.G. Freeman, B.D. Reiss, L. He, D.J. Peña, I.D. Walton, R. Cromer, C.D. Keating, M.J. Natan, Submicrometer metallic barcodes, Science 294 (2001) 137–141.
[3] E.E. McDonnell, S.L. Han, C. Hilty, K.L. Pierce, A. Pines, NMR analysis on microfluidic devices by remote detection, Anal. Chem. 77 (24) (2005) 8109–8114.
[4] E. Harel, A. Pines, Spectrally resolved flow imaging of fluids inside a microfluidic chip with ultrahigh time resolution, J. Magn. Reson. 193 (2) (2008) 199–206.
[5] S. Anwar, C. Hilty, C. Chu, L.-S. Bouchard, K.L. Pierce, A. Pines, Spin coherence transfer in chemical transformations monitored by remote detection NMR, Anal. Chem. 79 (7) (2007) 2806–2811.
[6] E. Harel, J. Granwehr, J.A. Seeley, A. Pines, Multiphase imaging of gas flow in a nanoporous material using remote-detection NMR, Nat. Mater. 5 (4) (2006) 321–327.
[7] V.S. Bajaj, J. Paulsen, E. Harel, A. Pines, Zooming in on microscopic flow by remotely detected MRI, Science 330 (2010) 1078–1081.
[8] A.J. Moulé, M.M. Spence, S.-I. Han, J.A. Seeley, K.L. Pierce, S. Saxena, A. Pines, Amplification of xenon NMR and MRI by remote detection, Proc. Nat. Acad. Sci. USA 100 (16) (2003) 9122–9127.
[9] C. Hilty, E.E. McDonnell, J. Granwehr, K.L. Pierce, S.-I. Han, A. Pines, Microfluidic gas-flow profiling using remote-detection NMR, Proc. Nat. Acad. Sci. USA 102 (42) (2005) 14960–14963.
[10] E. Harel, C. Hilty, K. Koen, E.E. McDonnell, A. Pines, Time-of-flight imaging of two-component flow inside a microfluidic chip, Phys. Rev. Lett. 98 (1) (2007) 017601.
[11] J. Granwehr, J.A. Seeley, Sensitivity quantification of remote detection NMR and MRI, J. Magn. Reson. 179 (2) (2006) 280–289.
[12] J. Paulsen, V.S. Bajaj, A. Pines, Compressed sensing of remotely detected MRI velocimetry in microfluidics, J. Magn. Reson. 205 (2) (2010) 196–201.
[13] N.W. Halpern-Manners, J.L. Paulsen, V.S. Bajaj, A. Pines, Remotely detected MRI velocimetry in microporous bead packs, J. Phys. Chem. A 115 (16) (2011) 4023–4030.
[14] T.Z. Teisseyre, J. Urban, N.W. Halpern-Manners, S.D. Chambers, V.S. Bajaj, F. Svec, A. Pines, Remotely detected NMR for the characterization of flow and fast chromatographic separations using organic polymer monoliths, Anal. Chem. 83 (15) (2011) 6004–6010.
[15] G. Zabow, S. Dodd, J. Moreland, A. Koretsky, Micro-engineered local field control for high-sensitivity multispectral MRI, Nature 453 (2008) 1058–1063.
[16] E. Kupce, J. Boyd, I.D. Campbell, Short selective pulses for biochemical applications, J. Magn. Reson. 106 (3) (1995) 300–303.
[17] J.M. Pope, S. Yao, Flow-selective pulse sequences, Magn. Reson. Imaging 11 (4) (1993) 585–591.
[18] E. Danieli, J.L. Mauler, J. Perlo, B. Blümich, F. Casanova, Mobile sensor for high-resolution NMR spectroscopy and imaging, J. Magn. Reson. 198 (1) (2009) 80–87.
[19] E. Danieli, J. Perlo, B. Blümich, F. Casanova, Small magnets for portable NMR spectrometers, Angew. Chem. Int. Ed. 49 (24) (2010) 4133–4135.
[20] E. Danieli, J. Perlo, B. Blümich, F. Casanova, Highly stable and finely tuned magnetic fields generated by permanent magnet assemblies, Phys. Rev. Lett. 110 (18) (2013) 180801.
[21] R. Kc, Y.N. Gowda, D. Djukovic, I.D. Henry, G.H.J. Park, D. Raftery, Susceptibility-matched plugs for microcoil NMR probes, J. Magn. Reson. 205 (1) (2010) 63–68.
[22] M. Takeda, K. Hallenga, M. Shigezane, M. Waelchi, F. Löhr, J.L. Markley, M. Kainosho, Construction and performance of an NMR tube with a sample cavity formed within magnetic susceptibility-matched glass, J. Magn. Reson. 209 (2) (2011) 167–173.